applied sciences

MDPI

Article

Cooperative Path Planning for Aerial Recovery of a UAV Swarm Using Genetic Algorithm and Homotopic Approach

Yongbei Liu [1], Naiming Qi [1,*], Weiran Yao [1,2], Jun Zhao [1] and Song Xu [1]

[1] School of Astronautics, Harbin Institute of Technology, Harbin 150001, China; liuyongbei@hit.edu.cn (Y.L.); yaoweiran@hit.edu.cn (W.Y.); zhaojun@hit.edu.cn (J.Z.); xusong92@hit.edu.cn (S.X.)

[2] Department of Mechanical and Industrial Engineering, University of Toronto, Toronto, ON M5S 3G8, Canada

* Correspondence: qinm@hit.edu.cn; Tel.: +86-0451-8641-8119

Received: 12 May 2020; Accepted: 14 June 2020; Published: 17 June 2020

Abstract: To maximize the advantages of being low-cost, highly mobile, and having a high flexibility, aerial recovery technology is important for unmanned aerial vehicle (UAV) swarms. In particular, the operation mode of "launch-recovery-relaunch" will greatly improve the efficiency of a UAV swarm. However, it is difficult to realize large-scale aerial recovery of UAV swarms because this process involves complex multi-UAV recovery scheduling, path planning, rendezvous, and acquisition problems. In this study, the recovery problem of a UAV swarm by a mother aircraft has been investigated. To solve the problem, a recovery planning framework is proposed to establish the coupling mechanism between the scheduling and path planning of a multi-UAV aerial recovery. A genetic algorithm is employed to realize efficient and precise scheduling. A homotopic path planning approach is proposed to cover the paths with an expected length for long-range aerial recovery missions. Simulations in representative scenarios validate the effectiveness of the recovery planning framework and the proposed methods. It can be concluded that the recovery planning framework can achieve a high performance in dealing with the aerial recovery problem.

Keywords: aerial recovery; UAV swarm; mother aircraft; recovery planning framework; genetic algorithm; homotopic approach

1. Introduction

High autonomy and large-scale swarms are two development trends of unmanned aerial vehicles (UAVs) [1,2]. However, UAV swarms can fly into enemy territory and sometimes they cannot safely return by themselves. In addition, their range is not sufficient to execute long-range missions. To overcome these shortcomings and to maximize the advantages of autonomous UAV swarms, especially to reduce the service cost and improve the reuse rate and efficiency, aerial recovery technology is important for UAV swarms. For insurance, the UAV swarm in the Gremlins program of the Defense Advanced Research Projects Agency has an operation mode called "launch-recovery-relaunch" [3]. In the future, this operation mode will become the mainstream for UAV swarms. In this operation mode, a mother aircraft is employed to deliver the UAVs to the designated locations for launch. Then, the mother aircraft recovers them after completing the missions and prepares to deliver them to the next locations. Compared with other UAV recovery methods on land or sea, aerial recovery has the greatest value, which can greatly expand the endurance and service time and comprehensively improve the flexibility and effectiveness of the

UAV swarms. However, there exist technical challenges because aerial recovery technology involves a variety of complex problems, including scheduling, path planning, rendezvous, and acquisition.

In recent years, some researchers have studied aerial recovery technologies for UAVs [4–7]. These studies focus on modeling the UAV recovery system and rendezvous guidance laws for the mother aircraft and the UAVs. The commonality between these works is that they focus on recovering a single UAV by the mother aircraft. With respect to the multi-UAV aerial recovery problem, it consists of two sub-problems: scheduling and path planning. Considering the dynamic constraints of UAVs and the recovery capability of the mother aircraft, scheduling and path planning of the multi-UAV aerial recovery problem will have high complexity and involve strong state information coupling. The recovery schedule and the recovery position series in the scheduling results will directly influence the performance of the path planning. Similarly, the rough path estimation can influence the scheduling process.

For the scheduling problem in the aerial recovery process, it has similarities with the traveling salesman problem with time windows [8,9], the vehicles routing problem with time windows [10], and the multi-robot recharging problem [11], which is considered from the perspective of combinatorial optimization. Many exact algorithms, such as the branch-and-bound algorithm [12,13], the cutting plane algorithm [14,15], integer linear programming [16,17], and dynamic programming [18,19], have been studied and applied to solve these problems at a small scale. However, the solution quantity will increase exponentially in large-scale combinatorial optimization problems. To solve such problems efficiently, many heuristic algorithms have been studied, including the genetic algorithm (GA) [20–22], the ant colony algorithm [23,24], the simulated annealing algorithm [25–27], and the tabu search algorithm [28,29].

Another major concern in the aerial recovery process is the usage of path planning to generate a path with an expected length for each UAV based on the scheduling results. Some researchers have considered path planning with an expected length. Meyer et al. studied the problem of intercepting a moving target with a Dubins vehicle at a given time, and they proposed three approaches, including a turning radius variation approach, a path deformation approach, and a final orientation rotation approach, to generate paths with an expected length [30]. Schumacher et al. proposed a line segment insertion approach to generate an ideal path for the task assignment problem with certain timing constraints [31]. Yao et al. proposed a homotopy-based approach to design an expected path by deforming specific Dubins paths for curvature-bounded vehicles [32]. Sun et al. presented a predictive-control-based algorithm to generate and track the path based on the requirements for the security and the path length for an unmanned surface vehicle [33]. In more general cases, Stodola proposed a smooth algorithm to connect a series of waypoints and generate a feasible path for UAVs in reconnaissance missions [34]. Shao et al. proposed a path planning method based on the particle swarm optimization algorithm on three dimensional UAV formation tasks [35]. Moreover, Thanh et al. solved the collision avoidance problem based on the combination of geometrical constraints and kinematics equations during the path planning process [36,37]. Cong et al. proposed a formation control algorithm based on the backstepping design method and a finite-time attitude tracking law to deal with the collision avoidance problem in path planning [38].

Although the existing works are effective in different situations, the aerial recovery problem of a UAV swarm has, to the authors' knowledge, not yet been researched. In this problem, the coupling mechanism between the scheduling and the path planning is bidirectional and it has not been elaborated. For recovery scheduling, an appropriate method should be proposed. Moreover, an effective path planning approach needs to be proposed and adopted to design the flight paths for the UAV swarm.

To address the above issues, we studied the aerial recovery problem of a UAV swarm by one mother aircraft. To describe the coupling mechanism between the scheduling process and the path planning process, a recovery planning framework is proposed. In the recovery planning framework, the outputs of the scheduling are delivered to the path planning to design the paths. Conversely, the intermediate results in path planning are treated as the feedback input for scheduling. A GA is employed to resolve the scheduling problem and generate the recovery position series and the

recovery path lengths owing to its convenience. Moreover, a homotopic approach is proposed for the path planning problem based on two different path homotopies. To validate the performance of the homotopic path planning approach and the recovery planning framework, a sufficient number of simulations for stochastic scenarios were conducted.

This paper is structured as follows. The preliminaries and the models of the aerial recovery problem are presented in Section 2. The recovery planning framework is proposed and introduced in Section 3. Section 4 presents the details of the genetic algorithm and the homotopic path planning approach in the recovery planning framework. Section 5 examines the proposed approaches and presents the overall performance of the recovery planning framework. Finally, Section 6 delivers the conclusions from this investigation and it describes our future research.

2. Preliminaries and Problem Statement

In this section, the mathematical models of the scheduling and path planning problem in the aerial recovery process are presented. For simplicity, the following assumptions are made:

1. Trajectory assumption. The trajectory of the mother aircraft is predefined and it is projected to a two dimensional plane for consideration. The aerial recovery process is considered to be a long-range mission and the execution time of the process is concerned with the mother aircraft trajectory.
2. Homogeneous assumption. UAVs in the swarm are homogeneous and fly at the same constant velocity, i.e., they can be recovered by the mother aircraft in an arbitrary sequence.
3. Recovery assumption. The mother aircraft employs the airborne actuators to recover the UAVs when they rendezvous at specified recovery positions with the same orientation in the sequence.
4. Communication assumption. The mother aircraft is always connected to the UAVs and the communication is perfect without delay and any other unfavorable factors.
5. Based on the assumptions, the schematic of the aerial recovery process is illustrated in Figure 1.

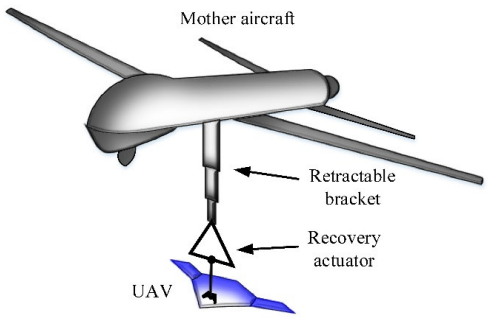

(**a**)

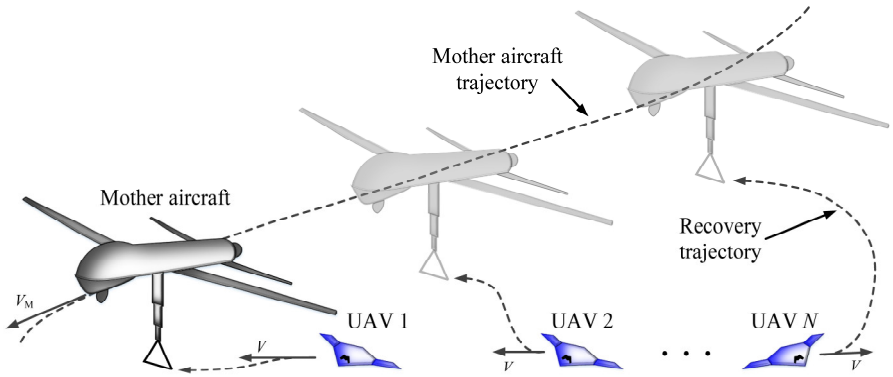

(**b**)

Figure 1. Schematic of the aerial recovery process. (**a**) Single-UAV recovery by using an airborne actuator on the mother aircraft. (**b**) Multi-UAV recovery (in an arbitrary sequence).

2.1. Recovery Scheduling

The scheduling problem is first formulated. Suppose that $\mathcal{N} \triangleq \{1, \ldots, N\}$ is the set of UAVs in the swarm. The mapping from the recovery serial number to the UAV index can be defined as:

$$i = g(s), \quad i, s \in \{1, 2, \ldots, N\} \tag{1}$$

where i is a UAV index; s is a recovery serial number; $S = (g(1), g(2), \ldots, g(N))$ represents a feasible recovery sequence of the aerial recovery problem.

In real-world applications, not all of the UAVs can be recovered by one mother aircraft because they have inappropriate positions or orientations and the mother aircraft has a limited recovery capability. Thus, the goal of the scheduling layer is to search for a recovery sequence to recover most UAVs as efficiently as possible. Two criteria are considered in this problem, namely, the number of recovered UAVs and the time cost of the aerial recovery process. The two objective functions can be given by

$$f_1(S) = \max \sum_{s=1}^{N} c_{sg(s)} \tag{2}$$

$$f_2(S) = \min t_N \tag{3}$$

subject to

$$c_{sg(s)} \in \{0,1\}, \quad \forall (s, g(s)) \in \mathcal{N} \times \mathcal{N}, \tag{4}$$

$$\sum_{s=1}^{N} c_{sg(s)} \le N, \tag{5}$$

$$t_N > \sum_{s=1}^{N} c_{sg(s)} \tau_{g(s)} \tag{6}$$

where $c_{sg(s)}$ indicates whether the UAV $g(s)$ can be recovered based on the serial number s; $\tau_{g(s)}$ is the recovery time cost taken by the mother aircraft to recover the UAV $g(s)$ and prepare for the next UAV; t_N indicates the whole time of the recovery process and it is given by

$$t_s = \begin{cases} \min\left(\left[t_{s-1}, +\infty\right) \cap W_{g(s)}\right) + \tau_{g(s)}, & \left[t_{s-1}, +\infty\right) \cap W_{g(s)} \neq \varnothing \\ t_{s-1}, & \text{otherwise} \end{cases} \tag{7}$$

subject to

$$t_0 = 0, \tag{8}$$

$$s \in \mathcal{N} \tag{9}$$

where $W_{g(s)}$ indicates the feasible recovery time window of UAV $g(s)$. To simplify the multi-objective optimization problem, the two objective functions can be normalized and combined by using the linear weighted method. The new objective function of the scheduling problem can be rewritten as

$$S^* = \arg\max_{S \in \mathbb{S}} \left(\alpha \times \left(f_1(S)/N\right) + \beta \times \left(\tau_{g(s)} \times f_1(S)/f_2(S)\right)\right) \tag{10}$$

subject to

$$\alpha + \beta = 1, \tag{11}$$

$$0 \le \alpha, \beta \le 1 \tag{12}$$

where $\mathbb{S}$ is the decision space that contains all of the feasible recovery sequences; α and β are the weight coefficients of the two objective values.

2.2. Path Planning

In this study, the UAVs are modeled as curvature-bounded vehicles and their kinemics are given by:

$$\begin{cases} \dot{x}_i = V\cos\varphi_i \\ \dot{y}_i = V\sin\varphi_i \\ \left|\dot{\varphi}_i\right| \le \mu_{\max} \end{cases}, \quad i \in \mathcal{N} \tag{13}$$

where x_i and y_i represent the coordinates of UAV i; V represents the flying speed of the UAVs; φ_i represents the heading angle of UAV i; $\mu_{\max}$ represents the maximum curvature of the heading angle.

To formulate the path planning problem, paths should be described correctly. Suppose that $T\mathbb{R}^2$ is the tangent bundle of $\mathbb{R}^2$ and $\boldsymbol{a} = (A, \vec{a})$, $\boldsymbol{b} = (B, \vec{b})$ are the two elements in $T\mathbb{R}^2$. Thus A, B are two points in $\mathbb{R}^2$ and $\vec{a}$, $\vec{b}$ are the corresponding velocity vectors, respectively. Given $\boldsymbol{a}, \boldsymbol{b} \in T\mathbb{R}^2$, the curve $p(z): [0, Z] \to \mathbb{R}^2$ is defined as a path that connects $\boldsymbol{a}$ and $\boldsymbol{b}$ for a UAV, and if the following conditions hold:

1. $\forall z \in [0, Z]$, $\left\|p'(z)\right\| = 1$, $\left\|p''(z)\right\| \le \mu_{\max}$.
2. $p(0) = A$, $p'(0) = \vec{a}$, $p(Z) = B$, $p'(Z) = \vec{b}$.
3. $p(z)$ is a continuous curve and it has a continuous first derivative.

As mentioned above, path planning is performed based on the recovery position series and the expected path length is generated in the recovery scheduling process. Given $S \in \mathbb{S}$ that is obtained in the scheduling layer, there exist

$$S \xrightarrow{\mathcal{S}} \mathbb{R}^+, \tag{14}$$

$$P \xrightarrow{\mathcal{L}} \mathbb{R}^{+} \tag{15}$$

where P indicates the set of flyable paths for a UAV; $\mathcal{S}$ represents the mapping from the recovery sequence to the lengths of the recovery paths; the function $\mathcal{L}$ represents the mapping from the paths in P to their lengths.

Based on the above definitions, the path planning process of a UAV focuses on searching for a curvature-bounded path with a minimum deviation from the expected path length when satisfying the boundary point constraints. Thus, the path planning problem can be formulated as

$$\min D\left(\mathcal{L}(p)\right) \tag{16}$$

subject to

$$\left(p(0), p'(0)\right) = \boldsymbol{a}, \tag{17}$$

$$\left(p\left(\mathcal{L}(p)\right), p'\left(\mathcal{L}(p)\right)\right) = \boldsymbol{b}, \tag{18}$$

$$\boldsymbol{a}, \boldsymbol{b} \in T\mathbb{R}^{2}, \tag{19}$$

$$p \in C\left(\boldsymbol{a}, \boldsymbol{b}\right) \tag{20}$$

where $D\left(\mathcal{L}(p)\right)$ is the length deviation of p from the expected value; $\boldsymbol{a}$ and $\boldsymbol{b}$ are the initial and recovery positions of the UAV, respectively; $C\left(\boldsymbol{a}, \boldsymbol{b}\right)$ is the set of all of the curvature-bounded paths that connect $\boldsymbol{a}$ and $\boldsymbol{b}$.

3. Recovery Planning Framework

When considering the prior studies that establish the interactive relationship between the sub-problems of complex problems [39–41], the recovery planning framework can be subdivided into two layers to describe the scheduling sub-problem and the path planning sub-problem. In this framework, the first layer is the scheduling and coordination module, and it acts as a decision maker. This module aims to find the optimal recovery sequence and generate the recovery position series and the expected recovery path lengths, and passes the solution to the next layer. The second layer, which is another major concern of this study, is the path planning module. The path planning module designs the desired paths with an expected length based on the recovery position series and the path lengths are obtained in the previous layer. Moreover, it generates and passes the control parameters to the control module of each UAV.

It is impractical to connect the scheduling layer and the path planning layer with a simple architecture because the two layers are coupled. The performance of the scheduling layer is affected by the path planning layer since the potential path estimation results can influence the results of the recovery time window calculation. On the contrary, the frequent path planning based on the results of the scheduling layer costs a considerable amount of time. To overcome these difficulties, the recovery planning framework is proposed, and it is shown in Figure 2.

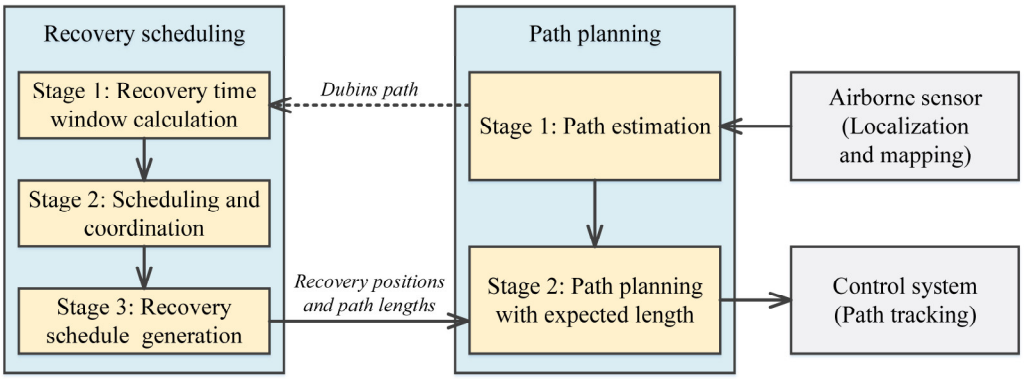

Figure 2. Recovery planning framework.

3.1. Recovery Scheduling Layer

The scheduling layer consists of three stages and the role of each stage is indicated as follows:

1. In stage 1, the recovery time windows of the UAV swarm are calculated. Since the flight path of the mother aircraft is predetermined, the position of the mother aircraft at any time is fixed. The basic idea of this stage is that when a UAV following a feasible path is capable of arriving at a position earlier than the mother aircraft, the arrival time of the mother aircraft is contained in the recovery time window of the UAV. The UAV can reach the position at this arrival time following a new path with a longer length, in order to rendezvous with the mother aircraft and facilitate a successful recovery.
2. In stage 2, the recovery sequence is optimized using a GA. Even with relatively few UAVs, finding the optimal recovery sequence is quite complicated. The GA is an efficient heuristic searching algorithm, and it is suitable enough to solve this scheduling problem. The execution process of the GA is given in Section 4.
3. In stage 3, the recovery schedule for the UAVs is generated based on the optimal recovery sequence, based on a similar iteration to Equation (7). Since the mother aircraft trajectory is predefined, the recovery positions on the mother aircraft trajectory can be obtained based on the recovery schedule. Further, the recovery path lengths for the UAVs are obtained since the velocity of the UAVs is known in advance. These results, at this stage, are directly passed to the path planning layer as the input.

3.2. Path Planning Layer

As the next step of the scheduling layer, the path planning layer consists of the path estimation stage and the path planning stage. The role of each stage is as follows:

1. In stage 1, the Dubins paths bridging the initial position of the UAV and each position of the predefined mother aircraft trajectory are generated based on a sample distance. Given the boundary constraints, the Dubins path was proven to be the shortest curvature-bounded path with the minimum flight time [42] and it has been applied extensively in path planning [43,44]. Combined with the above discussion for the recovery time windows, we can obtain the maximum recovery time window with the Dubins path. As shown in Figure 2, the path estimation results are passed back to the scheduling layer to calculate the recovery time windows.
2. In stage 2, the path with the expected length for each UAV is planned based on the recovery position and recovery path length. Only the Dubins path connecting the initial position and recovery position of a UAV is selected from stage 1 of this layer to construct the path homotopy. Then, the homotopic path planning approach is employed to generate a path with the expected length for the UAV. In the end, the related control parameters of the ideal path are transmitted to the control system for path tracking.

Overall, it can be seen from Figure 2 that stage 1 of the path planning layer is firstly executed depending on the information from the airborne sensors in the recovery planning framework. Then, the recovery scheduling layer runs according to the path estimation results. Next, stage 2 of the path planning layer is executed to generate a path with the expected length for each UAV, based on the recovery position and recovery path length obtained in the recovery scheduling layer. In the end, the trajectory control parameters are transmitted to the control module of each UAV.

4. Methodology

Based on the recovery planning framework, the GA is adopted to find the optimal recovery sequence, and a homotopic approach is proposed for path planning with the expected length. The details of the methods are presented and discussed in this section.

4.1. Genetic Algorithm

In this section, the GA is presented based on the specialty of the recovery scheduling problem. The GA begins by creating an original population based on the encoding method. Then the elite mechanism, the crossover operation, and the mutation operation are carried out to generate a new population. The execution process is terminated when reaching a maximum generation number N_g or achieving the optimal solution. Herein, the optimal solution in the last generation is the expected recovery sequence. The flow chart of the GA is demonstrated in Figure 3.

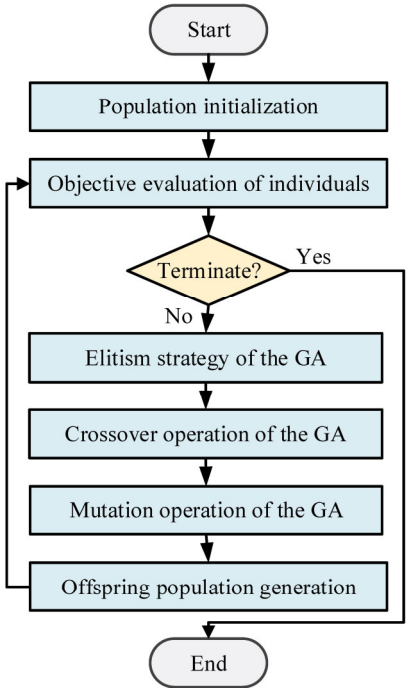

Figure 3. Flow chart of the genetic algorithm.

The core components of the GA that is employed in the recovery scheduling problem are explained in detail as follows:

1. Encoding. To accomplish the genetic operation, an effective representation of the chromosomes must be proposed. As discussed in the second section, each chromosome can be directly encoded by a recovery sequence S. The encoding method is, to a certain extent, similar to the path representation in the traveling salesman problem.

2. Initialization. In the GA, the searching space, which is called the population, is the collection of N_p recovery sequences. Utilizing the encoding method, the recovery sequences in the original population are randomly created to guarantee the diversity.
3. Objective evaluation. During the aerial recovery process, the UAVs need to keep a safe distance between each other to avoid collisions. The fitness value of each recovery sequence can be obtained from Equation (10) if the corresponding trajectories will not cause collisions. Conversely, the recovery sequences that will cause collisions are penalized with the "death penalty", i.e., they are given a fitness value of −1. Thus, these invalid recovery sequences are eliminated during the evolutionary process.
4. Elitism. In each generation, the best N_e recovery sequences form the elite group, and the elite group is copied to the next generation without any other genetic operations. By applying the elite mechanism, the good recovery sequences are reserved during the evolutionary process so that the optimal recovery sequence can be obtained faster.
5. Crossover. To perform the crossover operation, two recovery sequences are first selected based on the roulette wheel operator. The order crossover operator (OX1) is used to carry out the crossover operation due to its convenience [45] and the two recovery sequences are applied with the crossover operation, with a relatively high probability P_c. Figure 4 shows an example of the crossover operation. During the crossover operation, a sub-sequence is selected from one of the recovery sequences and it is copied to the same location of the offspring. Then, the other recovery serial numbers are filled with the same order as they appear in another recovery sequence starting from the second crossover point. The other offspring is created through the same process.
6. Mutation. The exchange mutation operator (EM) is selected to perform the mutation operation and each recovery serial number is affected by the mutation operator with a low probability P_m. As demonstrated in Figure 5, the mutated recovery serial number swaps its position with another randomly selected recovery serial number in the same recovery sequence.

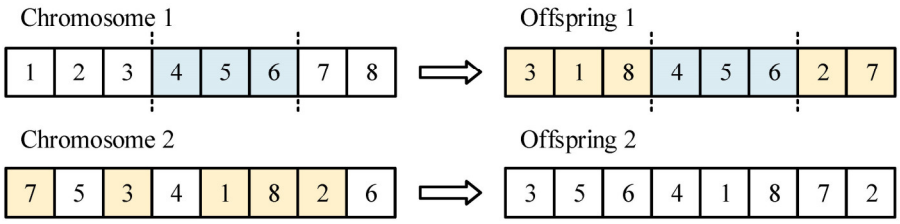

Figure 4. Example of the crossover operation.

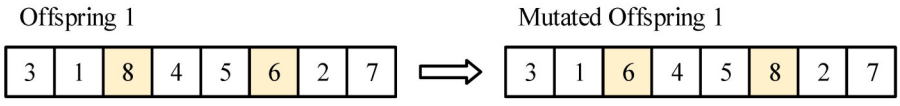

Figure 5. Example of the mutation operation.

4.2. Homotopic Path Planning Approach

In this section, a homotopic approach is proposed for planning paths with an expected length. Two path homotopy construction patterns are proposed and they are named as path homotopy 1 and path homotopy 2. In this investigation, the aerial recovery of the UAV swarm is considered to be a long-range mission. As a result, the Dubins path, which connects the initial position and recovery position of a UAV, is generated in stage 1 of the path planning layer and it contains both line and arc segments. Thus, we can only re-plan the line segment to generate the curvature-bounded paths with an expected length.

Suppose that $p_1, p_2 \in C(\boldsymbol{a}, \boldsymbol{b})$ are two curvature-bounded paths that connect $\boldsymbol{a}$ and $\boldsymbol{b}$. The continuous function H can be defined as a single-layer path homotopy if the following conditions hold:

1. $H(u):[0,1] \to E(p_1, p_2)$.
2. $H(0) = p_1$ and $H(0) = p_2$.
3. $E(p_1, p_2)$ is the space of all curvature-bounded paths between p_1 and p_2.

Thus, the output of the function $H(u)$ indicates a curvature-bounded path function within the path homotopy, and it can be given by

$$p = \mathcal{H}(\boldsymbol{a}, \boldsymbol{b}, u) = H(u) \tag{21}$$

where $\mathcal{H}$ is the mapping from the homotopic description to the path p. The role of the homotopic description is to reserve the boundary points and to use only one independent parameter u to describe the path. Moreover, for the convenience of computation, we can define another mapping as

$$p = \mathcal{T}(\boldsymbol{a}, \boldsymbol{q}) \tag{22}$$

where $\boldsymbol{q}=[\boldsymbol{q}_0 \quad \boldsymbol{q}_1 \quad \ldots \quad \boldsymbol{q}_M]$ indicates the controlling parameters of the path if the path satisfies $p = p_1 \cup p_2 \cup \ldots \cup p_M$. We can determine that the curvature vector $\boldsymbol{c}=[u_0 \quad u_1 \quad \ldots \quad u_M]$ and the length vector $\boldsymbol{l}=[l_0 \quad l_1 \quad \ldots \quad l_M]$ can be used to express the path, since the path consists of straight line segments and arc segments. Thus, the mapping can be rewritten as

$$p = \mathcal{T}(\boldsymbol{a}, \boldsymbol{c}, \boldsymbol{l}).. \tag{23}$$

where $\boldsymbol{q}_m = [\mu_m, \ l_m], \ m \in \{1, \ 2, \ \ldots, \ M\}$. Compared with the homotopic description, the ending boundary point in this description is not reserved; hence, it is obtained by iteration. However, this description is much more intuitive to express the path.

Based on these two path descriptions, two path homotopy construction patterns are presented for the path planning. As shown in Figure 6, the axis defined by the line segment of the Dubins path divides the plane into two half planes. For simplicity, path homotopy 1 is in the upper plane and it is the first to be considered. It can be observed that path homotopy 1 consists of a curve and a straight line, and the curve consists of four equal arcs. Based on the geometrical relationship, the boundary conditions of path homotopy 1 can be denoted as

$$H(0) = \mathcal{T}(\boldsymbol{a}, \boldsymbol{c}_0, \boldsymbol{l}_0), \tag{24}$$

$$H(1) = \mathcal{T}(\boldsymbol{a}, \boldsymbol{c}_1, \boldsymbol{l}_1), \tag{25}$$

$$\boldsymbol{c}_0 = [\mu_a \quad \mu_{\text{trans0}} \quad -\mu_{\text{trans0}} \quad \mu_{\text{trans0}} \quad \mu_b], \tag{26}$$

$$\boldsymbol{c}_1 = [\mu_a \quad 0 \quad 0 \quad 0 \quad \mu_b], \tag{27}$$

$$\boldsymbol{l}_0 = \left[l_a \quad \frac{\arcsin(\mu_{\text{trans0}} l/4)}{\mu_{\text{trans0}}} \quad \frac{2\arcsin(\mu_{\text{trans0}} l/4)}{\mu_{\text{trans0}}} \quad \frac{\arcsin(\mu_{\text{trans0}} l/4)}{\mu_{\text{trans0}}} \quad l_b \right], \tag{28}$$

$$\boldsymbol{l}_1 = [l_a \quad l/4 \quad l/2 \quad l/4 \quad l_b] \tag{29}$$

where μ_{trans0} is the curvature bound of the arcs in the curve; μ_a and μ_b are the curvatures of arc segments along the Dubins path; l is the length of the line segment along the Dubins path; l_a and l_b are the lengths of arc segments along the Dubins path.

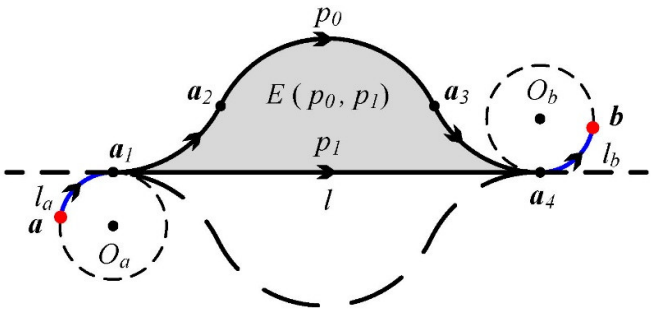

Figure 6. Path homotopy 1.

On this basis, $H(u)$ indicates a path with a curvature vector $\boldsymbol{c}=[\mu_a \quad \mu_{\text{trans}} \quad -\mu_{\text{trans}} \quad \mu_{\text{trans}} \quad \mu_b]$ for the arbitrary $u \in (0,1)$. To describe this path, a linear function between u and $\boldsymbol{c}$ can be defined as

$$\mu_{\text{trans}} = (1-u)\mu_{\text{trans0}} \quad , \quad u \in (0,1). \tag{30}$$

Based on the definition of path homotopy 1 and the geometrical relationship, there exists $\mu_{\text{trans0}} = 4/l$. Since $\boldsymbol{a}$, $\boldsymbol{b}$ and the curvature vector $\boldsymbol{c}$ are known variables, the length vector $\boldsymbol{l}$ can be obtained by iteration. Moreover, path homotopy 1 in the lower half plane can also be constructed, and the paths within this path homotopy are described in a similar way.

To cover all of the lengths of the curvature-bounded path, another path homotopy is proposed. As shown in Figure 7, path homotopy 2 consists of circles. Based on the geometrical relationship, the boundary conditions of path homotopy 2 in the upper half plane can be written as

$$H(0) = \mathcal{T}(\boldsymbol{a}, \boldsymbol{c}_0, \boldsymbol{l}_0), \tag{31}$$

$$H(1) = \mathcal{T}(\boldsymbol{a}, \boldsymbol{c}_1, \boldsymbol{l}_1), \tag{32}$$

$$\boldsymbol{c}_0 = [\mu_a \quad 0 \quad \mu_{\text{trans0}}/2 \quad 0 \quad \mu_b], \tag{33}$$

$$\boldsymbol{c}_1 = [\mu_a \quad 0 \quad \mu_{\text{trans0}} \quad 0 \quad \mu_b], \tag{34}$$

$$\boldsymbol{l}_0 = [l_a \quad l_1 \quad 4k\pi/\mu_{\text{trans}} \quad l_2 \quad l_b], \quad k \in \mathbb{N}^+, \tag{35}$$

$$\boldsymbol{l}_1 = [l_a \quad l_1 \quad 2k\pi/\mu_{\text{trans}} \quad l_2 \quad l_b], \quad k \in \mathbb{N}^+, \tag{36}$$

$$l_1 + l_2 = l \tag{37}$$

where l_1 and l_2 are the lengths of two line segments, and k represents the lap number of the circles.

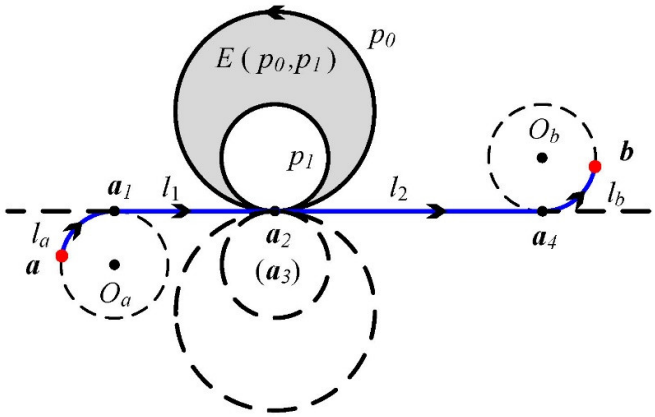

Figure 7. Path homotopy 2.

Similarly, $H(u)$ indicates a path with a curvature vector $\boldsymbol{c}=[\mu_a \quad 0 \quad \mu_{\text{trans}} \quad 0 \quad \mu_b]$ for the arbitrary $u \in (0,1)$. To describe this path, a linear function between u and $\boldsymbol{c}$ can be defined as

$$\mu_{\text{trans}} = \left(\frac{u}{2}+\frac{1}{2}\right)\mu_{\text{trans0}} \quad , \quad u \in (0,1). \tag{38}$$

Since the UAVs are modeled as curvature-bounded vehicles, there exists $\mu_{\text{trans0}} = \mu_{\max}$. Then, the length vector l can be obtained by iteration as well. As before, path homotopy 2 in the lower half plane can be constructed and the paths within this path homotopy are described in a similar way.

Based on the two path homotopy construction patterns, the curvature-bounded paths within the homotopy are described. In particular, the path varies monotonously based on u, so that the path with the expected length can be planned by solving Equation (16) using the Newton–Raphson iterative method.

5. Simulation Results

To verify the performance of the recovery planning framework, representative simulations were conducted using MATLAB. The simulations in this section are divided into three major parts. First, the path coverage evaluation of the homotopic path planning approach in long-range missions was carried out. Then, the verification of the recovery scheduling process was conducted. In the end, the overall performance of the multi-UAV recovery planning framework was validated for stochastic scenarios. A Monte Carlo study that considered the quantity of the UAVs is also presented.

5.1. Evaluation of the Path Length Coverage

The path length coverage of the homotopic approach is discussed through simulations in the representative scenarios. To evaluate the homotopic approach, the path length coverage interval is used. It is calculated by subtracting the shortest curvature-bounded path length; that is, the Dubins path length, from the planned path length using the homotopic approach. In the simulations, the initial position and the recovery position are taken into consideration since the planned path is affected by the boundary points. The initial coordinate of the UAV is fixed at (−25,0) and the heading angle is 135°. Moreover, the heading angle of the trajectory of the mother aircraft is separately set as 45°, 135°, −135°, and −45°. The recovery positions on the trajectories of the mother aircraft are 32.5 km and 50 km away from the initial position of the UAV, respectively. Moreover, the minimum turning radius of the UAV is set to 2 km^{-1}.

The settings of the recovery positions are listed in Table 1 and the simulation results are shown in Figure 8. As demonstrated, the Dubins path is used as the initial curvature-bounded path. The paths

are generated by using the homotopic approach, and then the path length coverage of the homotopic approach can be obtained.

Table 1. Settings of the recovery positions.

Index	Coordinate of the Recovery Position (km)	Heading Angle of the Recovery Position (Degree)
(**a**)	(12.5,0)	45
(**b**)	(12.5,0)	135
(**c**)	(12.5,0)	−135
(**d**)	(12.5,0)	−45
(**e**)	(25,0)	45
(**f**)	(25,0)	135
(**g**)	(25,0)	−135
(**h**)	(25,0)	−45

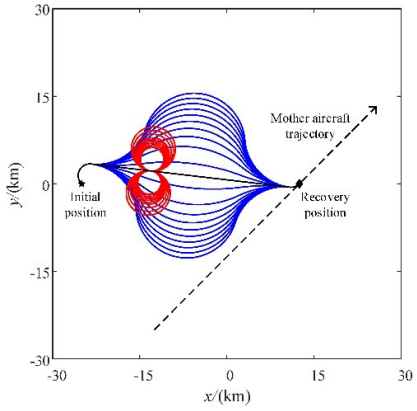

(**a**)

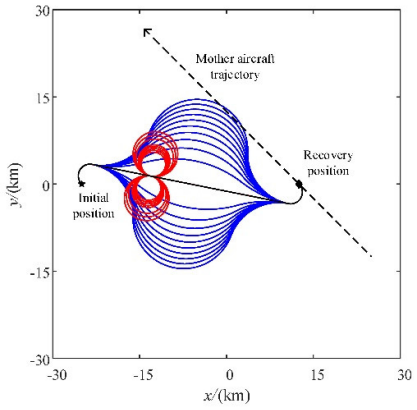

(**b**)

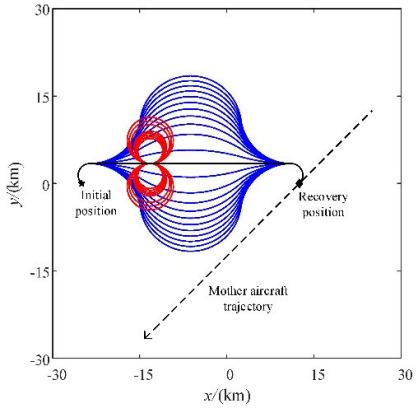

(**c**)

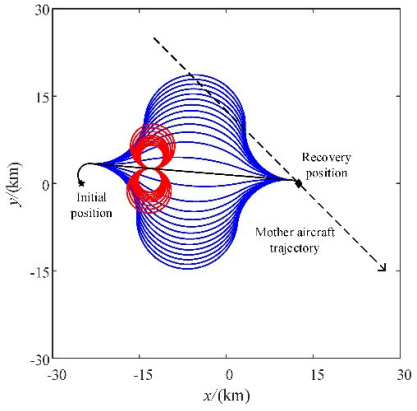

(**d**)

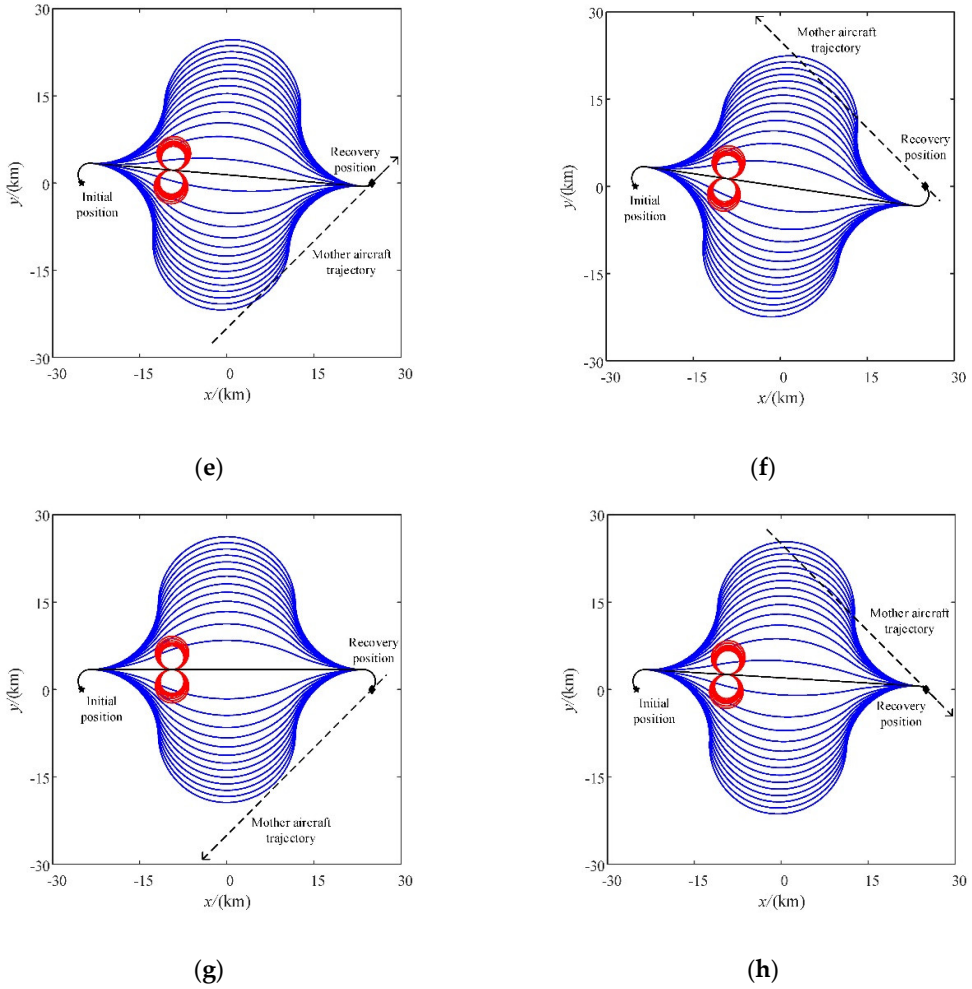

Figure 8. Paths generated using the homotopic approach. (**a**–**d**) The coordinates of the recovery position are (12.5,0) and the heading angles are 45°, 135°, −135°, and −45°; (**e**–**h**) The coordinates of the recovery position are (25,0) and the heading angles are 45°, 135°, −135°, and −45°.

The path length coverage intervals under the different conditions are given in Table 2. For each case in the simulations, we can find that all of the expected path lengths can be covered by using a combination of the two path homotopies.

Table 2. Path length coverage interval.

Index	Path Length Coverage Interval of Path Homotopy 1 (km)	Path Length Coverage Interval of Path Homotopy 2 (km)
(**a**)	[0, 19.63]	[12.56, +∞)
(**b**)	[0, 19.70]	[12.56, +∞)
(**c**)	[0, 19.76]	[12.56, +∞)
(**d**)	[0, 19.83]	[12.56, +∞)
(**e**)	[0, 26.79]	[12.56, +∞)
(**f**)	[0, 26.84]	[12.56, +∞)
(**g**)	[0, 26.89]	[12.56, +∞)
(**h**)	[0, 26.94]	[12.56, +∞)

As we can see, the path length coverage interval of path homotopy 1 ranges from zero to its maximum value, and path homotopy 2 ranges from its minimum value to positive infinity. To ensure that all of the path lengths are covered based on the two path homotopies, the maximum path length coverage value of path homotopy 1 needs to be greater than the minimum path length coverage value of path homotopy 2. Based on the geometrical relationship, we can get $l > 4\pi/\left[(\pi-2)\mu_{\max}\right]$ if l is the length of the straight line segment of the Dubins path. Since the aerial recovery of the UAV swarm is considered to be a long-range mission, the above condition is satisfied so that all of the path lengths are covered based on the two path homotopies.

5.2. Verification of the Recovery Scheduling

To verify the recovery scheduling process, representative simulations are conducted. In this section, simulations are carried out in a scenario of 100 km × 100 km and the trajectory of the mother aircraft is fixed. The sample distance of the mother aircraft trajectory is 0.1 km. The velocity of each UAV is 100 m/s and the curvature bound is 2 km^{-1}. The velocity of the mother aircraft is 150 m/s and the recovery time cost τ of each UAV is 60 s. For more intuitive simulation results, three UAVs are set to be recovered by the mother aircraft. The settings of the UAVs, including the initial position and the initial direction, are given in Table 3.

Table 3. Initial settings of the UAVs.

UAV Index	Initial Position (km)	Initial Direction (Degree)
1	(8,52)	11.25
2	(80,65)	56.25
3	(10,30)	−90

Figure 9 shows the simulation results of the recovery scheduling. As seen in Figure 9a–c, the UAVs are simply recovered at the minimum value for their recovery time windows. When the mother aircraft recovers all of the UAVs, the recovery scheduling is executed and the optimal recovery sequence is (2,3,1). In Figure 9d, the recovery trajectory of UAV 1 is different to that in Figure 9a. The recovery process of UAV 1 is influenced by UAV 3 since the recovery process cannot be performed instantly. Figure 10 intuitively illustrates the timeline of the recovery process. In particular, the recovery time window of UAV 3 consists of two regions due to the geometric relationship between its initial position and the recovery position. Moreover, the results show that the minimum value of the recovery time window of UAV 1 is occupied by the recovery time cost of UAV 3; hence, UAV 1 is immediately recovered after completing the recovery process of UAV 3. In this case, the recovery scheduling process is simple, but it can be difficult when the size of the UAV swarm increases. The recovery processes of the UAVs can influence each other. In addition, UAVs with multi-region recovery time windows do not necessarily need to be recovered urgently and

other UAVs that are in need should be preferentially taken into account. As discussed in the previous sections, the GA is adopted to deal with the large-scale scheduling problem.

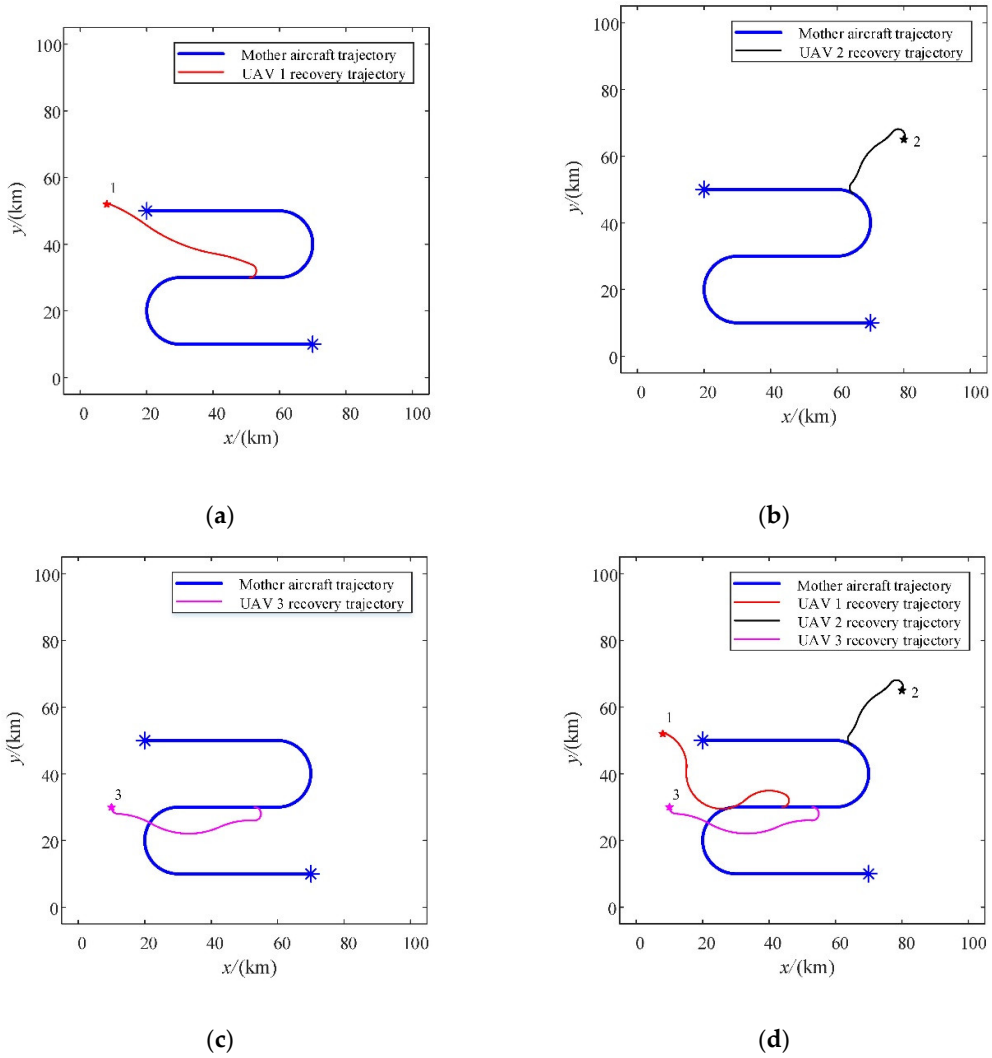

Figure 9. Simulation results of the recovery scheduling. (**a**) Recover UAV 1 individually; (**b**) Recover UAV 2 individually; (**c**) Recover UAV 3 individually; (**d**) Recover UAV 1, UAV 2, and UAV 3.

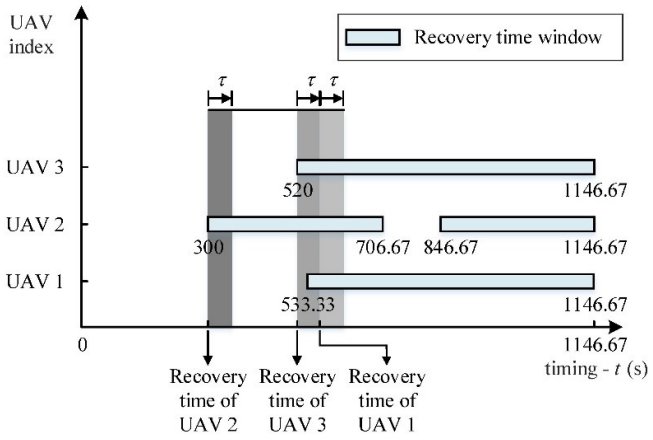

Figure 10. Recovery time of UAV 1, UAV 2, and UAV 3 when recovering all of them.

5.3. Overall Performance of the Recovery Planning Framework

In this section, simulations are carried out in a scenario that is 200 km × 200 km to validate the overall performance of the recovery planning framework. The size of the UAV swarm is set to 10, 20, and 30, respectively. The settings of the UAVs are listed in Table 4. Similarly, the velocity of each UAV is 100 m/s and the curvature bound is 2 km^{-1} in these simulations. The trajectory of the mother aircraft consists of straight-line segments and arc segments. The sample distance of the mother aircraft trajectory is 0.1 km. The flying velocity of the mother aircraft is 150 m/s and the recovery time cost τ of each UAV is 60 s. The coefficients α and β are set as 0.5 since they are equally important. When considering the GA that is used in the scheduling problem, the parameters are given in Table 5.

Table 4. Initial settings of UAVs.

UAV Index	Initial Position (km)	Initial Direction (degree)
1	(112.14,8.81)	−126.32
2	(15.92,33.11)	76.14
3	(58.20,53.44)	2.34
4	(80.60,139.85)	−166.28
5	(196.66,14.64)	126.41
6	(47.16,143.79)	85.46
7	(110.57,149.48)	100.87
8	(66.92,67.88)	−175.92
9	(62.24,89.75)	14.43
10	(64.45,10.75)	168.71
11	(67.24,166.73)	125.25
12	(109.31,92.17)	−170.33
13	(122.10,177.38)	−113.12
14	(3.52,41.84)	−24.50
15	(64.07,110.61)	106.88
16	(147.39,9.81)	116.26
17	(138.77,155.22)	11.44
18	(146.05,62.70)	−68.80
19	(178.55,82.65)	130.13
20	(108.69,154.81)	−31.60
21	(145.63,34.32)	90.13
22	(194.31,109.47)	−104.30
23	(34.63,180.37)	23.16
24	(173.51,179.49)	98.03
25	(38.05,27.44)	−62.11
26	(199.72,62.28)	116.80
27	(95.72,187.33)	41.86
28	(45.29,171.27)	−47.51
29	(78.91,66.34)	−42.99
30	(33.04,150.45)	2.809

Table 5. Parameters of the GA.

Parameter	N_g	N_p	N_e	P_c	P_m
Value	3000	100	3	0.95	0.01

Figure 11 presents the simulation results of the recovery planning framework. As demonstrated in Figure 11a, four UAVs do not have recovery time windows when the mother aircraft is a non-maneuvering target, because they are too close to the initial position of the mother aircraft or

they have unsuitable heading angles. The rest of the UAVs can be recovered by the mother aircraft successfully. In Figure 11b, all 10 UAVs can be recovered when the mother aircraft is a maneuvering target. Based on the recovery planning framework, the optimal recovery sequence, along with the recovery position series and the recovery path lengths, are obtained. The flyable paths of the UAV swarm are designed and generated using the homotopic path planning approach, where the path homotopy is selected according to the geometrical relationship. Figure 11c,d shows the simulation results when 10 new UAVs join the UAV swarm. It can be observed that, as before, the recovery planning framework performs well. Figure 11e,f illustrates the performance of the recovery planning framework when 10 new UAVs once again join the UAV swarm. As shown in Figure 11e, 10 UAVs do not have recovery time windows. Moreover, 19 of the UAVs can be recovered and 1 UAV cannot be recovered. In Figure 11f, all of the UAVs in the scenario can be recovered by the maneuvering mother aircraft and the paths with the expected lengths are designed for the UAVs. As demonstrated, the recovery planning framework performs well even though the size of the UAV swarm increases. Figure 12 shows the distances from the UAVs to the mother aircraft in these simulations. As the figure shows, the results validate the effectiveness of the homotopic path planning approach since the flyable paths of the UAVs can be designed and generated for recovery.

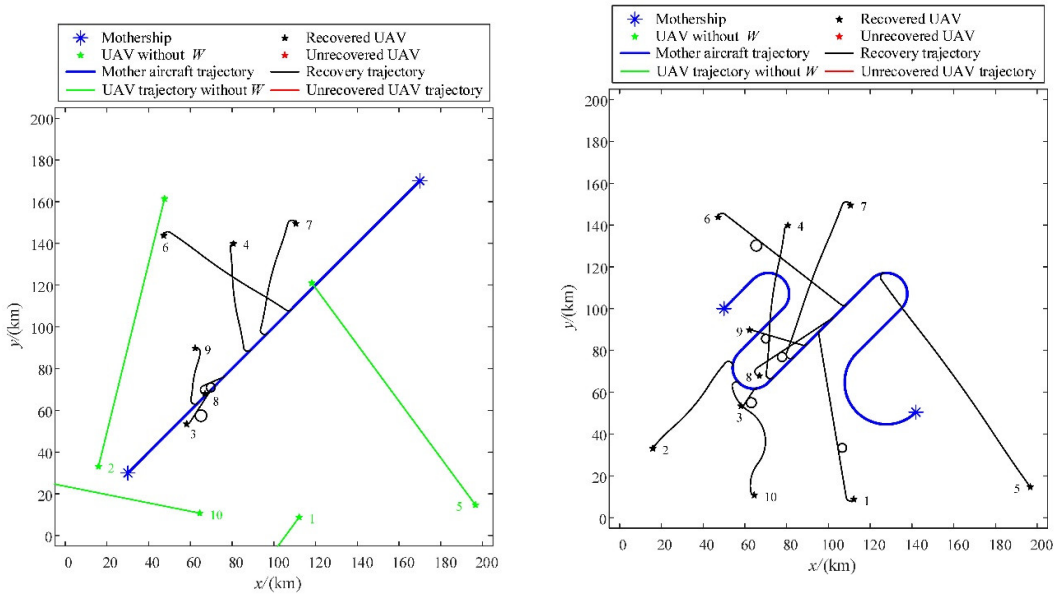

(**a**) (**b**)

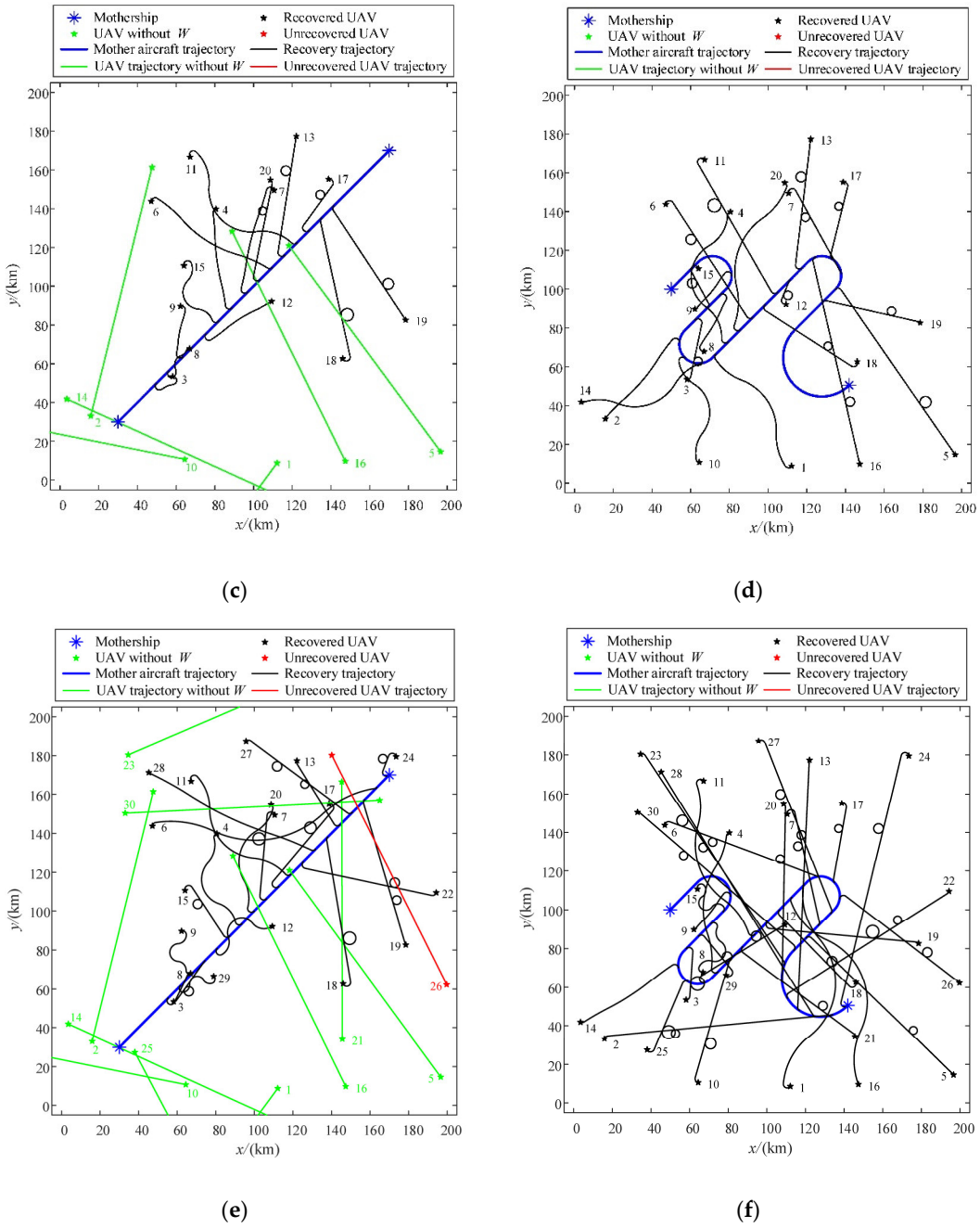

Figure 11. Representative recovery results. (**a**) 10 UAVs with a non-maneuvering mother aircraft; (**b**) 10 UAVs with a maneuvering mother aircraft; (**c**) 20 UAVs with a non-maneuvering mother aircraft; (**d**) 20 UAVs with a maneuvering mother aircraft; (**e**) 30 UAVs with a non-maneuvering mother aircraft; (**f**) 30 UAVs with a maneuvering mother aircraft.

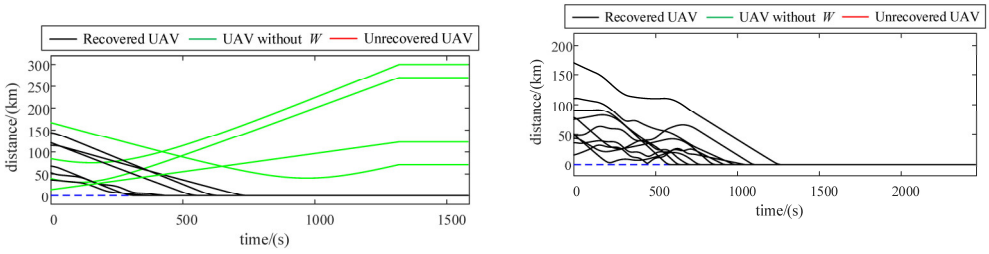

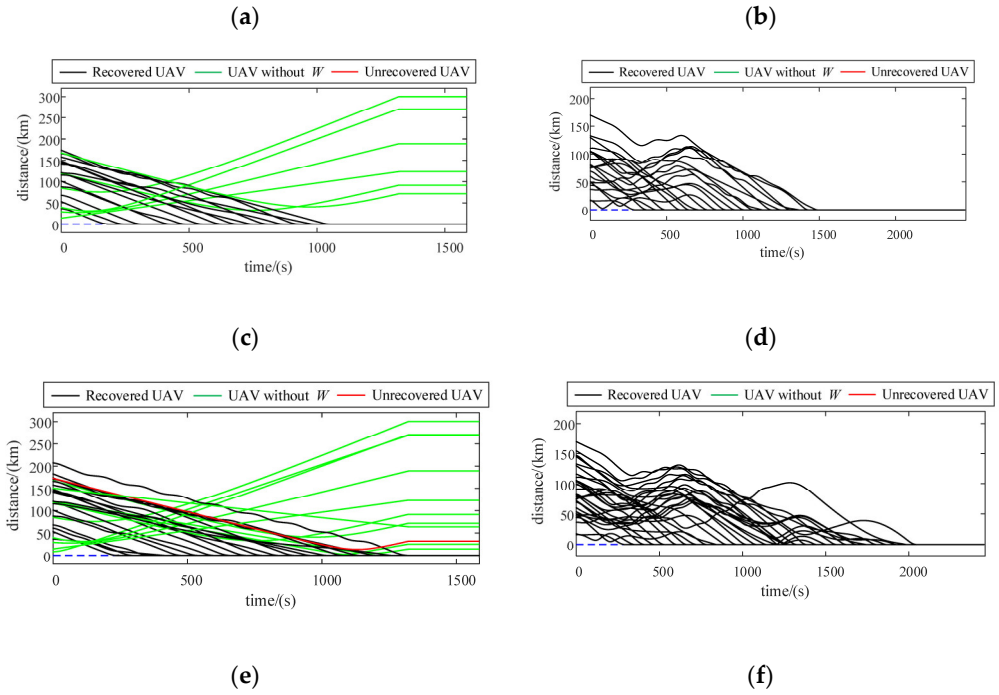

Figure 12. Distances from the UAVs to the mother aircraft. (**a**) 10 UAVs with a non-maneuvering mother aircraft; (**b**) 10 UAVs with a maneuvering mother aircraft; (**c**) 20 UAVs with a non-maneuvering mother aircraft; (**d**) 20 UAVs with a maneuvering mother aircraft; (**e**) 30 UAVs with a non-maneuvering mother aircraft; (**f**) 30 UAVs with a maneuvering mother aircraft.

In addition, a Monte Carlo study is carried out for further validation. The configuration of the UAV swarm and the trajectory of the mother aircraft is the same as the previous simulation. In each case, the Monte Carlo simulation performs 100 runs. The results of the mean value, the standard deviation, and the best value of the objective function is shown in Table 6. Clearly, the mean values with a non-maneuvering mother aircraft are lower than those with a maneuvering mother aircraft, respectively. This is caused by the inappropriate distances and the heading angles of the UAVs, so that they do not have recovery time windows. Besides, the mean values are close to the best values, which indicates that the UAVs can be recovered efficiently by using the recovery planning framework. In addition, we can see that there is a slight increase in the standard deviation as the size of the UAV swarm increases, but they are in an ideal range. Overall, the results of the Monte Carlo study further validate that the recovery planning framework has a good performance in the aerial recovery problem for the UAV swarm. This framework ensures that the mother aircraft recovers the most UAVs in the most efficient manner despite the quantity change for the UAVs, and the flyable paths of the UAV swarm can be designed by using the homotopic path planning approach.

Table 6. Results of the Monte Carlo study.

Objective Value [1]	Non-Maneuvering Mother Aircraft			Maneuvering Mother Aircraft		
	$N = 10$	$N = 20$	$N = 30$	$N = 10$	$N = 20$	$N = 30$
Mean	52.56	72.82	71.50	72.66	88.65	90.77
St Dev	0	0	1.73	0	0.35	2.29
Best	52.56	72.82	73.66	72.66	89.22	92.97

[1] All of the objective values should be multiplied by 10^{-2}.

6. Conclusions

In this paper, the multi-UAV aerial recovery problem with a single mother aircraft is examined. A recovery planning framework is proposed to establish the coupling mechanism between the scheduling layer and the path planning layer. In the recovery planning framework, the outputs of the scheduling layer are delivered to the path planning layer to design paths. Conversely, the path estimation stage in the path planning layer is treated as the feedback input to the scheduling layer to obtain the maximum recovery time window for each UAV. A GA is introduced to optimize the recovery sequence. Based on the GA, the recovery planning framework can realize efficient and precise scheduling for the UAV swarm. Moreover, a homotopic approach, which searches paths of the expected length within a certain homotopy, is proposed for the path planning of the UAV swarm. Two path homotopy construction patterns based on deforming the line segment of the Dubins path have been presented in detail. The simulation results show that all of the paths with expected lengths are covered in a long-range aerial recovery by using the homotopic path planning approach. Then, the recovery scheduling process is verified in a representative scenario. Furthermore, the simulation results validate the overall performance of the recovery planning framework. In conclusion, this framework can ensure that the mother aircraft recovers the most UAVs in the most efficient manner despite the quantity change of the UAVs.

Future work based on the findings from this research will include an investigation on extending the path homotopy construction patterns to a generalized form. By doing this, the proposed homotopic path planning approach can be applied to more complicated situations. Then, aerial recovery with multiple mother aircrafts will be considered to improve the effectiveness of the UAV swarms even further. Moreover, it is necessary to focus on the aerial recovery problem with the unknown mother aircraft trajectories in advance, since the motions of the mother aircrafts are difficult to obtain in the real world. To make the summary and conclusion more sufficient and convincing, experiments on a real system which employs the aerial recovery planning framework can also be considered in the future.

Author Contributions: Methodology, Y.L. and W.Y.; software, Y.L. and W.Y.; validation, Y.L., S.X., and J.Z.; formal analysis, Y.L. and S.X.; investigation, Y.L. and N.Q.; writing—Original draft preparation, Y.L. and J.Z.; writing—Review and editing, W.Y. and N.Q. All authors have read and agreed to the published version of the manuscript.

Funding: This research received no external funding.

Acknowledgments: The authors would like to thank the editors and reviewers for their hard work and valuable suggestions that improved this paper substantially.

Conflicts of Interest: The authors declare no conflict of interest.

References

1. Wu, H.S.; Li, H.; Xiao, R.B.; Liu, J. Modeling and simulation of dynamic ant colony's labor division for task allocation of UAV swarm. *Physica A* **2018**, *491*, 127–141.
2. Huang, S.A.; Teo, R.S.H.; Kwan, J.L.P.; Liu, W.Q. Distributed UAV Loss Detection and Auto-replacement Protocol with Guaranteed Properties. *J. Intell. Robot. Syst.* **2019**, *93*, 303–316.
3. Gremlins. Available online: https://www.darpa.mil/program/gremlins (accessed on 3 May 2020).
4. Sun, L.; Beard, R.W.; Colton, M.B.; McLain, T.W. Dynamics and control of cable-drogue system in aerial recovery of micro air vehicles based on Gauss's principle. In Proceedings of the American control conference, St. Louis, MO, USA, 10–12 June 2009 (accessed on 9 April 2020).
5. Sun, L.; Beard, R.W.; Colton, M.B. Motion planning and control for mothership-cable-drogue systems in aerial recovery of micro air vehicles. In Proceedings of the American control conference, Baltimore, MD, USA, 30 June–2 July 2010 (accessed on 15 April 2020).
6. Sun, L.; Beard, R.W. Towed-body trajectory tracking in aerial recovery of micro air vehicle in the presence of wind. In Proceedings of the American control conference, San Francisco, CA, USA, 29 June–1 July 2011 (accessed on 11 April 2020).

7. Carlson, D.C.; Colton, M.B. Out-of-plane orbit estimation and tracking for aerial recovery of micro air vehicles. In Proceedings of the IEEE international conference on robotics and automation, Anchorage, AK, USA, 3–8 May 2010 (accessed on 3 April 2020).
8. Dumas, Y.; Desrosiers, J.; Gelinas, E.; Solomon, M.M. An optimal algorithm for the traveling salesman problem with time windows. *Oper. Res.* **1995**, *43*, 367–371.
9. Balas, E.; Simonetti, N. Linear time dynamic-programming algorithms for new classes of restricted TSPs: A computational study. *INFORMS J. Comput.* **2001**, *13*, 56–75.
10. Desrochers, M.; Desrosiers, J.; Solomon, M.M. A new optimization algorithm for the vehicle routing problem with time windows. *Oper. Res.* **1992**, *40*, 342–354.
11. Mathew, N.; Smith, S.L.; Waslander, S.L. Multirobot Rendezvous Planning for Recharging in Persistent Tasks. *IEEE Trans. Robot.* **2015**, *31*, 128–142.
12. D'Ariano, A.; Pacciarelli, D.; Pranzo, M. A branch and bound algorithm for scheduling trains in a railway network. *Eur. J. Oper. Res.* **2007**, *183*, 643–657.
13. Qin, H.; Zhang, Z.Z.; Lim, A.; Liang, X.C. An enhanced branch-and-bound algorithm for the talent scheduling problem. *Eur. J. Oper. Res.* **2016**, *250*, 412–426.
14. Kis, T.; Kova´cs, A. A cutting plane approach for integrated planning and scheduling. *Comput. Oper. Res.* **2012**, *3*, 320–327.
15. Karimi-Nasab, M.; Seyedhoseini, S.M. Multi-level lot sizing and job shop scheduling with compressible process times: A cutting plane approach. *Eur. J. Oper. Res.* **2013**, *231*, 598–616.
16. Tahar, D.N.; Yalaoui, F.; Chu, C.B.; Amodeo, L. A linear programming approach for identical parallel machine scheduling with job splitting and sequence-dependent setup times. *Int. J. Prod. Econ.* **2006**, *99*, 63–73.
17. Montero, A.; Méndez-Díaz, I.; Miranda-Bront, J.J. An integer programming approach for the time-dependent traveling salesman problem with time windows. *Comput. Oper. Res.* **2017**, *88*, 280–289.
18. Yang, J.B. GA-based discrete dynamic programming approach for scheduling in FMS environments. *IEEE Trans. Syst. Man Cybern. Part B-Cybern.* **2001**, *31*, 824–835.
19. Jin, Z.P.; Shima, T.; Schumacher, C.J. Optimal Scheduling for Refueling Multiple autonomous aerial vehicles. *IEEE Trans. Robot.* **2006**, *22*, 682–693.
20. Shima, T.; Rasmussen, S.J.; Sparks, A.G.; Passino, K.M. Multiple task assignments for cooperating uninhabited aerial vehicles using genetic algorithms. *Comput. Oper. Res.* **2006**, *33*, 3252–3269.
21. Wei, H.J.; Li, S.B.; Jiang, H.M.; Hu, J.; Hu, J.J. Hybrid genetic simulated annealing algorithm for improved flow shop scheduling with makespan criterion. *Appl. Sci.* **2018**, *8*, 2621.
22. Liu, Y.B.; Qi, N.M.; Yao, W.R.; Liu, Y.F.; Li, Y. Optimal scheduling for aerial recovery of multiple unmanned aerial vehicles using genetic algorithm. *Proc. Inst. Mech. Eng. Part G-J. Aerosp. Eng.* **2019**, *233*, 5347–5359.
23. Gajpal, Y.; Rajendran, C. An ant-colony optimization algorithm for minimizing the completion-time variance of jobs in flowshops. *Int. J. Prod. Econ.* **2006**, *101*, 259–272.
24. Vlachos, A. Ant Colony System algorithm solving a Thermal Generator Maintenance Scheduling Problem. *J. Intell. Fuzzy Syst.* **2013**, *24*, 713–723.
25. Ponnambalam, S.G.; Jawahar, N.; Aravindan, P. A simulated annealing algorithm for job shop scheduling. *Prod. Plan. Control* **1999**, *10*, 767–777.
26. Cruz-Chávez, M.A.; Martınez-Rangel, M.G.; Cruz-Rosales, M.H. Accelerated simulated annealing algorithm applied to the flexible job shop scheduling problem. *Int. Trans. Oper. Res.* **2017**, *24*, 1119–1137.
27. Cruz-Chávez, M.A.; Peralta-Abarca, J.C.; Cruz-Rosales, M.H. Cooperative Threads with Effective-Address in Simulated Annealing Algorithm to Job Shop Scheduling Problems. *Appl. Sci.* **2019**, *9*, 3360.
28. Shutler, P.M.E. A priority list based heuristic for the job shop problem: Part 2 tabu search. *J. Oper. Res. Soc.* **2004**, *55*, 780–784.
29. Raza, S.A.; Akgunduz, A.; Chen, M.Y. A tabu search algorithm for solving economic lot scheduling problem. *J. Heuristics* **2006**, *12*, 413–426.
30. Meyer, Y.; Isaiah, P.; Shima, T. On Dubins paths to intercept a moving target. *Automatica* **2015**, *53*, 256–263.
31. Schumacher, C.; Chandler, P.R.; Rasmussen, S.J.; Walker, D. Path Elongation for UAV Task Assignment. In Proceedings of the AIAA Guidance, Navigation, and Control Conference, Austin, TX, USA, 11–14 August 2003.

32. Yao, W.R.; Qi, N.M.; Zhao, J.; Wan, N. Bounded curvature path planning with expected length for Dubins vehicle entering target manifold. *Robot. Auton. Syst.* **2017**, *97*, 217–229.
33. Sun, X.J.; Wang, G.F.; Fan, Y.S.; Mu, D.D.; Qiu, B.B. An Automatic Navigation System for Unmanned Surface Vehicles in Realistic Sea Environments. *Appl. Sci.* **2018**, *8*, 193.
34. Stodola, P. Route Optimization for Cooperative Aerial Reconnaissance. In Modelling and Simulation for Autonomous Systems, Rome, Italy, 24–26 October 2017.
35. Shao, S.K.; Peng, Y.; He, C.L.; Du, Y. Efficient path planning for UAV formation via comprehensively improved particle swarm optimization. *ISA Trans.* **2020**, *97*, 415–430.
36. Thanh, H.L.N.N.; Hong, S.K. Completion of Collision Avoidance Control Algorithm for Multicopters Based on Geometrical Constraints. *IEEE Access* **2018**, *6*, 27111–27126.
37. Ha, L.N.N.T.; Bui, D.H.P.; Hong, S.K. Nonlinear Control for Autonomous Trajectory Tracking While Considering Collision Avoidance of UAVs Based on Geometric Relations. *Energies* **2019**, *12*, 1551.
38. Cong, Y.Z.; Du, H.B.; Jin, Q.C.; Zhu, W.W.; Lin, X.Z. Formation control for multiquadrotor aircraft: Connectivity preserving and collision avoidance. *Int. J. Robust Nonlinear Control* **2020**, *30*, 2352–2366.
39. Vachtsevanos, G.; Tang, L.; Drozeski, G.; Gutierrez, L. From mission planning to flight control of unmanned aerial vehicles: Strategies and implementation tools. *Annu. Rev. Control* **2005**, *29*, 101–115.
40. Shanmugavel, M.; Tsourdos, A.; White, B.; Żbikowski, R. Co-operative path planning of multiple UAVs using Dubins paths with clothoid arcs. *Control Eng. Pract.* **2010**, *18*, 1084–1092.
41. Yao, W.R.; Qi, N.M.; Wan, N.; Liu, Y.B. An iterative strategy for task assignment and path planning of distributed multiple unmanned aerial vehicles. *Aerosp. Sci. Technol.* **2019**, *86*, 455–464.
42. Dubins, L.E. On curves of minimal length with a constraint on average curvature, and with prescribed initial and terminal positions and tangents. *Am. J. Math.* **1957**, *79*, 497–516.
43. Manathara, J.G.; Ghose, D. Rendezvous of multiple UAVs with collision avoidance using consensus. *J. Aerosp. Eng.* **2012**, *25*, 480–489.
44. Wang, Y.; Wang, S.; Tan, M.; Zhou, C.; Wei, Q.P. Real-time dynamic Dubins-Helix method for 3-D trajectory smoothing. *IEEE Trans. Control Syst. Technol.* **2014**, *23*, 730–736.
45. Larranaga, P.; Kuijpers, C.M.H.; Murga, R.H.; Inza, I.; Dizdarevic, S. Genetic algorithms for the travelling salesman problem: A review of representations and operators. *Artif. Intell. Rev.* **1999**, *13*, 129–170.